ANALYSIS OF SHEAR-INDUCED PLATELET AGGREGATION WITH POPULATION BALANCE MATHEMATICS

THOMAS K. BELVAL AND J. DAVID HELLUMS
Biomedical Engineering Laboratory, Rice University, Houston, Texas 77251

ABSTRACT Suspensions of blood platelets aggregate and degranulate when subjected to a shearing flow of sufficient intensity. This work examines, by means of a population balance technique, the kinetics of platelet aggregation in a shear field. The particle collision efficiency, ϵ, and the particle void volume fraction, ϕ, are estimated from particle number density data. The collision efficiency respresents the fraction of particle collisions that result in the binding together of the involved particles. We term ϵ and ϕ population balance properties because they refer to physical characteristics of platelets and aggregates that are pertinent to their aggregation behavior. Experiments focused on the dependence of ϵ on platelet concentration, shearing rate, and time in a controlled shear field. The collision efficiency is lower in dilute platelet suspensions. This finding supports an ADP-mediated mechanism for shear aggregation. The collision efficiency passes through a maximum with respect to shearing rate, suggesting a competition between the opposing effects of increasing platelet activation and increasing collision violence. The collision efficiency is highest during the first ten seconds in the shear field and declines significantly thereafter. Even at its maximum, however, ϵ for shear aggregation is small: only about one in every thousand particle collisions results in binding.

INTRODUCTION

A fluid in motion near a solid surface experiences shearing stress because the surface retards the fluid's motion. Certain abnormal conditions can elevate shearing stress in blood. Shearing stresses near artificial heart valves, for example, can be many times higher than normal physiologic levels.

Elevated shearing stresses in blood can profoundly affect blood cells. Leukocytes release lysosomal enzymes in a shear field and exhibit increased adhesiveness and impaired chemotaxis and phagocytosis after shear stress exposure (Martin et al., 1979). Erythrocytes become less deformable following shear stress exposure (O'Rear et al., 1982). Platelets undergo perhaps the most striking changes: they degranulate (Brown et al., 1975; Johnston et al., 1975; Anderson et al., 1978*a*) and aggregate (Anderson et al., 1978*a*; Johnston et al., 1975) in a shear field. Following shear stress exposure, platelet aggregation in response to chemical stimuli is altered (Anderson et al., 1978b; Hellums and Hardwick, 1981).

Our study examines the kinetics of platelet aggregation in a shear field both experimentally and mathematically. The experimental program focuses on three variables: shearing rate, platelet concentration, and time in the shear field. We employ population balance mathematics to interpret particle number density data from the shear aggregation experiments. The population balance technique estimates properties of platelets and aggregates that are pertinent to their aggregation kinetics. For example, this technique gives a numerical estimate of platelet-platelet binding affinity. The population balance properties offer insights into the dynamic state of platelets aggregating in a shear field. Moreover, the properties provide a concise means of describing the detailed evolution of particle number density over time for shear aggregation.

EXPERIMENTAL

This paper emphasizes a mathematical treatment of aggregation measurements obtained by experiment. Hence, we offer only an abridged description of our experimental methods. A more detailed account of the experimental work appears in Belval et al. (1984) or Belval (1984). The experimental procedure has three steps: (*a*) preparing the platelet suspension; (*b*) applying a shear field to the suspension; and (*c*) measuring the resulting aggregation.

Blood was obtained from healthy adult volunteers by venipuncture and was anticoagulated with sodium heparin (10 units/ml blood). Centrifuging the blood at 150 *g* yielded a platelet-rich plasma (PRP) supernatant. The PRP was secured in air-tight containers to inhibit alkalosis. Part of the PRP received a second centrifugation at 15,000 *g* to prepare platelet-free plasma (PFP). Mixing the appropriate volumes of PRP and PFP yielded a platelet suspension with the target platelet concentration for the experiment.

A cone-plate viscometer applied the shear field to the platelet suspension. The principle of operation for the viscometer is simple: rotating the cone while the plate remains stationary imposes a shearing motion to a fluid specimen sandwiched between them. We employed a truncated cone with an angle of 1°, giving a gap between the cone and plate that ranged

Thomas K. Belval is now with the Health Care Division, Monsanto Company, St. Louis, MO 63167.

from 90 μm at the center to 610 μm at the outside. The design of the viscometer permits accurate control of the shearing rate, a measure of the intensity of the shearing motion. In our study, the shearing rate ranged from 100 s^{-1} to 10,000 s^{-1}, and the exposure time of the platelet suspension in the shear field was between 10 s and 2 min.

Platelet aggregation in the shear field was assessed by tracking changes in the particle size distribution of the platelet suspension. A sample of the platelet suspension before exposure to the shear field provided a baseline particle size distribution. Additional samples taken while the viscometer was running (through a hole drilled in the plate) gave a time sequence of how platelet aggregation changes the particle size distribution from the baseline condition. An electronic particle counter (Coulter Electronics, Model ZBI with Channelyzer) measured the particle size distribution of the samples. The electronic particle counter generates a one-hundred–bar histogram depicting number frequency vs. particle volume (Fig. 1). The area under the histogram is proportional to the total number of particles measured.

A microcomputer (Apple II Plus) interfaced to the electronic particle counter made a record of the histograms obtained from the viscometer samples. Additional programs on the computer allowed us to obtain the average of replicate histograms, deduct background noise, calculate histogram statistics, plot histograms, and convert number density histograms to volume density histograms. Volume density histograms depict the distribution of total particle volume across the one-hundred particle volume categories.

THE POPULATION BALANCE

Basic Equations

Population balances predict how the makeup of a collection of particles changes as a result of interactions among particles and interactions between particles and the surrounding medium. In a population balance, a particle number density function mathematically expresses the makeup of a collection of particles. The arguments of the number density function can be any particle parameter, for example, particle volume. Solving the population balance determines the number density function as it evolves in time.

For platelet aggregation in a uniform shear field, the appropriate population balance is the laminar shear coalescence equation (Drake, 1972),

$$\partial n(v, t)/\partial t = \int_{v_s}^{v/2} k_G(w, v - w)\, n(w, t)\, n(v - w, t)\, dw - \int_{v_s}^{\infty} k_G(w, v)\, n(w, t)\, n(v,t)\, dw, \quad (1)$$

where $0 \leq t < \infty$, $v_s \leq v < \infty$. The laminar shear coalescence equation is a special case of the general population balance in which aggregation is the only form of interaction between particles. Eq. 1 does not consider particle breakup.

Eq. 1 is an integro-differential equation for $n(v, t)$, the particle number density with respect to particle volume, v, at time, t, after the onset of aggregation. The differential, $n(v, t)\, dv$, represents the number of particles (per unit volume of suspension) with volumes between v and $v + dv$. Hence, the total number of particles at any time is,

$$N(t) = \int_{v_s}^{\infty} n(v, t)\, dv, \quad (2)$$

where v_s is the volume of the smallest particle in the suspension.

The expression $k_G(w, v)$ in Eq. 1 is a collision frequency factor, called the laminar shear coalescence kernel, for particle aggregation in laminar shearing flow. Smoluchowski (1917) derived the following expression for the

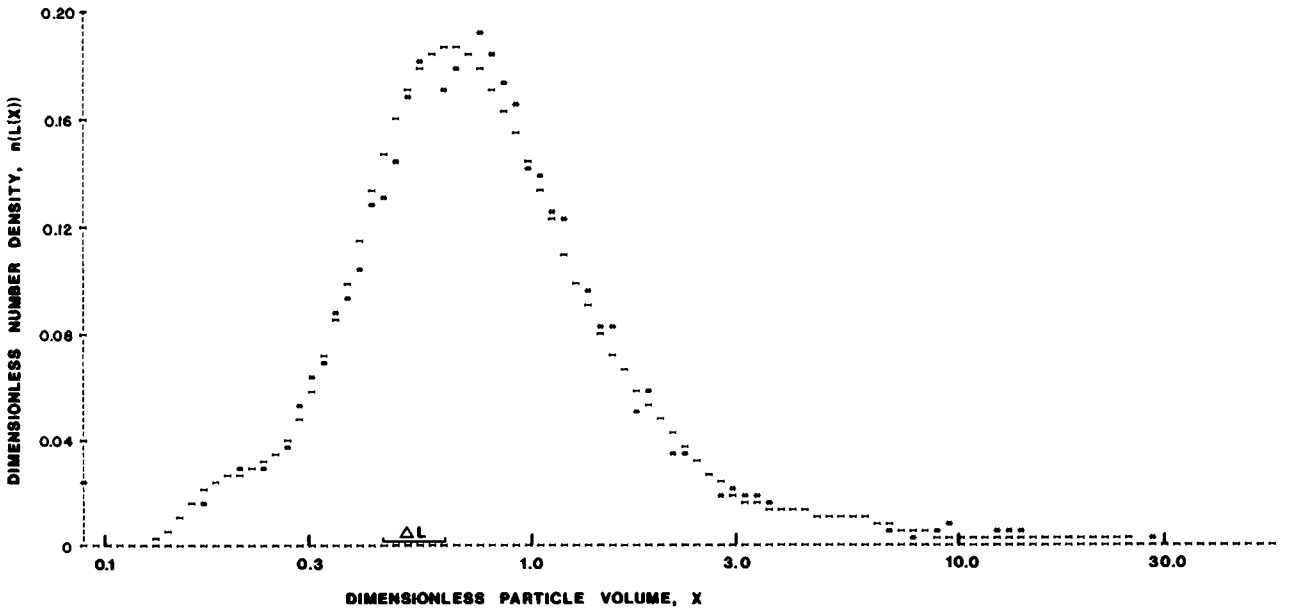

FIGURE 1 (*) Example of a particle number density histogram from shear aggregation. Each point corresponds to a specific particle volume category. (I) A cubic spline interpolate of the measured histogram.

laminar shear coalescence kernel,

$$k_G(w, v) = \frac{G}{\pi}\left[w^{1/3} + v^{1/3}\right]^3, \tag{3}$$

where G is the shearing rate. As Eq. 3 reveals, $k_G(w, v)$ is a symmetric function of w and v, the volumes of the two colliding particles.

Although mathematically complex, Eq. 1 expresses a simple balance: the rate of accumulation of particles of a given size equals their rate of formation minus their rate of disappearance. The left side of Eq. 1 represents the time rate of change of the number of particles with volume v. The first term on the right side of Eq. 1 describes the rate of formation of particles with volume v by the collision and binding together of two particles whose volumes add up to v. The second term represents the rate of disappearance of particles with volume v by their collision and binding with a particle of any volume. Restricting the upper limit of the first integral to $v/2$ prevents counting each combination of particles more than once.

Dimensionless Transformation

Dimensionless transformation of Eq. 1 yields a more convenient form of the coalescence equation for numerical computations and for comparison with experiment. The following definitions convert the variables of Eq. 3 to dimensionless form

$$X = v/v_o, \tag{4}$$

$$T = GN_o v_o t/\pi, \tag{5}$$

$$n(X, T) = v_o n(v, t)/N_o, \tag{6}$$

$$a_G(X, Y) = \frac{\pi}{Gv_o} k_G(v, w). \tag{7}$$

Eq. 4 defines the dimensionless particle volume, X, and Eq. 5 defines the dimensionless time, T. Eq. 6 renders the particle number density function dimensionless. Note that $n(X, T)$ and $n(v, t)$ are different functions, not the same function with different arguments. Eq. 7 defines a dimensionless version of the laminar shear coalesence kernel. Here, Y is a dummy argument that corresponds to w in Eq. 3. In the above definitions, v_o refers to the mean particle volume of $n(v, 0)$, the initial particle number density function, and N_o represents the total number of particles per unit volume of suspension at time $t = 0$. Introducing the definitions into Eq. 1 and simplifying yields a dimensionless form of the laminar shear coalesence equation,

$$\partial n(X, T)/\partial T = \int_{X_s}^{X/2} a_G(Y, X - Y)\, n(Y, T)\, n(X - Y, T)\, dY - \int_{X_s}^{\infty} a_G(Y, X)\, n(Y, T)\, n(X, T)\, dY, \tag{8}$$

where $X_s \leq X < \infty$ and $0 \leq T < \infty$. In dimensionless form, Eq. 3 simplifies to

$$a_G(X, Y) = [X^{1/3} + Y^{1/3}]^3. \tag{9}$$

Note that Eqs. 8 and 9 contain only a single parameter, X_s. As a result, the solution to Eq. 8 pertains to any particle concentration, N_o, shearing rate, G, or mean initial particle volume, v_o. Only a different initial condition, $n(X, 0)$, will change the form of the solution, $n(X, T)$.

Although dimensionless, $n(X, T)$ remains awkward to manipulate because X ranges over several orders of magnitude. Replacing X with a logarithmic scale, $L(X)$, compresses the numerical range to more manageable limits

$$L(X) = \ln (X/X_s)/\ln 2. \tag{10}$$

The sequence $X = X_s, 2X_s, 4X_s, 8X_s, 16X_s, \ldots$ now corresponds to $L = 0, 1, 2, 3, 4, \ldots$. Eq. 11 relates $n(L, T)$ to $n(X, T)$,

$$n(L, T) = Xn(X, T) \ln 2. \tag{11}$$

The dimensionless laminar shear coalescence equation in terms of L is given by Belval (1984).

MODIFYING THE POPULATION BALANCE

Introducing $\epsilon(T)$ and $\phi(X)$

The laminar shear coalescence kernel of Smoluchowski (1917), Eq. 9, contains two assumptions that are inappropriate for platelet aggregation. First, the kernel assumes the particles are spheres. A corollary to this assumption is that particles coalesce after binding to form a new, larger sphere. Platelets, however, are not spherical. They are prolate ellipsoids with an average aspect ratio of about 3:1 (Frojmovic and Panjwani, 1976). Moreover, platelet aggregates take on a variety of irregular shapes and can contain significant void space (Born and Hume, 1967). They are not tightly packed spheres. Second, the laminar shear coalescence kernel assumes all particle collisions to result in the binding together of the involved particles. Experimental evidence, however, indicates that a significant fraction of platelet collisions are unsuccessful (Karino and Goldsmith, 1979; Chang and Robertson, 1976; Bell and Goldsmith, 1984) even at low shearing rates and in the presence of added ADP.

We devised population balance properties, simple functions of time or particle volume, to address the improper assumptions behind Eq. 9 by modifying the laminar shear coalescence kernel. An acceptable set of properties should improve upon the laminar shear coalescence equation as a model for shear aggregation kinetics. Our yardstick for measuring improvement is the reduction in the histogram error, given by Eq. 12

$$E_i = \frac{\| n[L, T_i] - n_c(L, T_i) \|}{\| n_c(L, T_i) \|}, \qquad i = 0, 1, 2, \ldots . \tag{12}$$

Here, the T_i represent the sampling times for a shear aggregation experiment. The $\|\cdot\|$ operator in Eq. 12 performs a sum of squares calculation. For example

$$\| n_c(L, T_i) \| = \sum_{k=1}^{100} n_c(L_k, T_i)^2, \tag{13}$$

where the L_k ($k = 1, 2, \ldots, 100$) are the dimensionless volumes corresponding to each of the one hundred histogram bars. The numerator of Eq. 12 is a measure of the difference between the model prediction, $n[L, T_i]$, and a cubic-spline fit of the observed particle number density, $n_c(L, T_i)$. Note that [ ] indicate a model prediction whereas ( ) denote an observed histogram.

We proposed and tested a number of modified coalescence kernels containing different population balance properties designed to relax the questionable restrictions of Eq. 9. Among those tested, the expression below gave good results with minimal changes to Eq. 9

$$a_{G\epsilon\phi}(X, Y) = \epsilon(T)\, a_G\left(\frac{X}{1 - \phi(X)}, \frac{Y}{1 - \phi(Y)}\right), \tag{14}$$

where

$$\phi(X) = \begin{cases} 0, & X < 2 \\ \phi_a, & X \geq 2 \end{cases} \tag{15}$$

and $0 \leq \epsilon(T) \leq 1$, $0 \leq \phi(X) < 1$. As the notation $a_{G\epsilon\phi}$ indicates Eq. 14 introduces two population balance properties to the laminar shear coalescence kernel: $\epsilon(T)$, the particle collision efficiency; and $\phi(X)$, the particle void volume fraction. The collision efficiency expresses the likelihood that particles will bind together upon colliding. Introducing $\epsilon(T)$ relaxes the assumption that all particle collisions must succeed. The particle void fraction is, as the name indicates, the fraction of a particle's volume that is void space. Introducing $\phi(X)$ relaxes the assumption that particles must coalesce to spheres upon binding.

A mathematical definition for $\epsilon(T)$ follows from substituting $a_{G\epsilon\phi}$ into Eq. 8 and dividing by $\epsilon(T)$,

$$\frac{\partial n(X, T)}{\epsilon(T)\partial T} = \int_{X_s}^{X/2} a_{G\phi}(Y, X - Y)\, n(Y, T)\, n(X - Y, T)\, dY - \int_{X_s}^{\infty} a_{G\phi}(Y, X)\, n(Y, T)\, n(X, T)\, dY, \tag{16}$$

where

$$a_{G\phi}(X, Y) = a_G\left(\frac{X}{1 - \phi(X)}, \frac{Y}{1 - \phi(Y)}\right). \tag{17}$$

The form of Eq. 16 suggests a new time scale, T', such that $dT' = \epsilon(T)\, dT$ and $T' = 0$ when $T = 0$. From inspection, Eq. 16 in terms of T' describes an aggregation process wherein every collision succeeds. For an incremental drop in particle population occurring over time dT,

$$\epsilon(T) = dT'/dT, \tag{18}$$

where dT' represents the differential time required for the same incremental drop in population if every collision succeeds.

In Eq. 14, total particle volume, $X/[1 - \phi(X)]$, replaces "packed" particle volume, X, in the arguments of a_G. Thus, Eq. 14 accounts for the expanded collision diameter of particles containing void space. Eq. 15 defines $\phi(X)$ as a simple step function. All particles with dimensionless volumes below $X = 2$ are "single platelets" and have zero void volume. All particles larger than $X = 2$ are "aggregates" with the same void volume fraction, ϕ_a.

Determining $\epsilon(T)$ and $\phi(X)$ from Experimental Observations

Applying Eq. 14 to analyze platelet aggregation in a shear field involves estimating $\epsilon(T)$ and $\phi(X)$ for a particular experiment. Our estimation scheme attempts to define $\epsilon(T)$ and $\phi(X)$ such that the sum of the E_i, $i = 1, 2, \ldots$ is a minimum. An iterative approach is necessary:

(*a*) Fit a Gaussian curve to $n(L, O)$, the initial platelet number density histogram. An example is given in Fig. 2.

(*b*) Select a trial value for ϕ_a and numerically solve Eq. 8 using $a_{G\phi}$ (Eq. 17) as the coalescence kernel. The equations are expressed in terms of the variable L (Eqs. 10 and 11) for solution.

(*c*) Calculate the time-average of $\epsilon(T)$ for each time interval between number density measurements, $n(L, T_i)$, $i = 0, 1, 2, \ldots$.

(*d*) Evaluate the sum of the E_i, $i = 0, 1, 2, \ldots$.

(*e*) Select a new value for ϕ_a and repeat the sequence of steps, starting at step two, until the sum of the histogram errors reaches a minimum or is sufficiently small.

Fig. 3 illustrates the effects of ϵ and ϕ by comparing the appearance of numerical solutions with number density functions obtained by experiment. Note that the solution for the unmodified coalescence kernel is indistinguished from the abscissa.

This solution predicts that essentially no singlets remain, in marked contrast to the experimental curve. Introducing $\epsilon(T)$ gives much better results, as illustrated by the curve designated by "*E*." This case forces the total populations to agree by slowing the theoretical pace of aggregation. However, there are still more small aggregates ($2 < X < 10$) and fewer singlets than the observations. Including both $\epsilon(T)$ and $\phi(X)$ in the coalescence kernel further improves the agreement, as shown by the curve designated by "*V*." By accounting for the void space within aggregates, this solution predicts more frequent collisions involving aggregates (their collision diameter is now larger). Small aggregates incorporate into larger aggregates more rapidly but their rate of production from single platelets will not change. As a result, curve "*V*" predicts fewer small aggregates and more singlets than solution

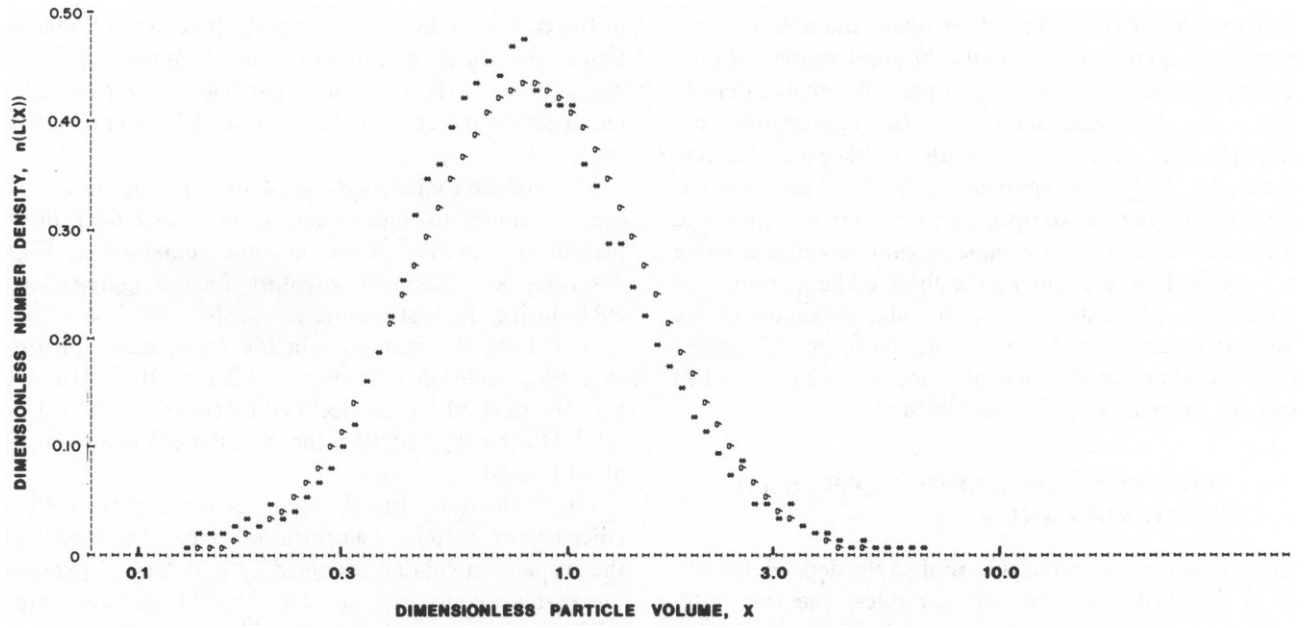

FIGURE 2 Example showing Gaussian approximation (9) vs. platelet number density histogram (*). The best choice among three Guassian curves was $\sigma = 0.9$, yielding a histogram error of $E = 0.08$. Both histograms have the same average particle volume and dimensionless population.

"E," and better agrees with the appearance of the observed histogram.

Both the particle size measurements and the coalescence equation are based on particle number density. Transforming number density data to volume density can reveal additional information about the larger aggregates. Eq. 19 relates dimensionless volume density, $v(L, T)$, to dimensionless number density, $n(L, T)$,

$$v(L, T) = X(L)\, n(L, T). \tag{19}$$

Whereas the area under a number density curve corre-

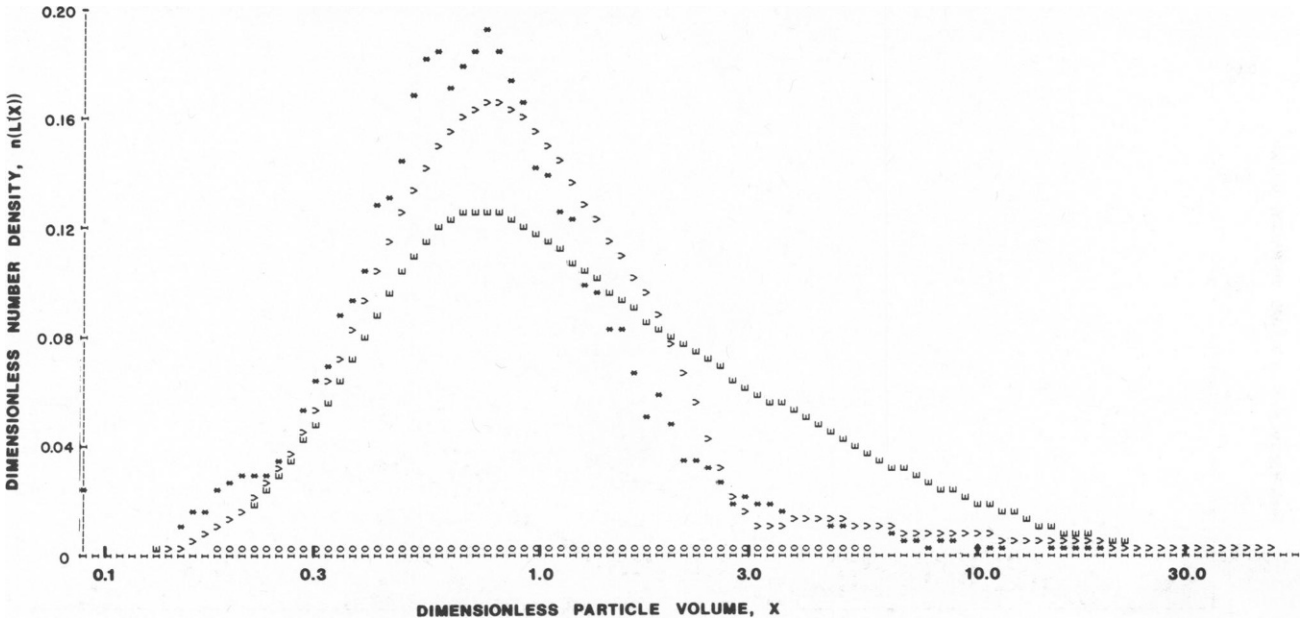

FIGURE 3 Example of how $\epsilon(T)$ and $\phi(X)$ improve coalescence equation predictions for an intermediate stage of shear aggregation ($P = 0.43$): (*) histogram for PRP following 60 s exposure at $G = 5{,}000\ s^{-1}$; (0) predicted histogram without $\epsilon(T)$ or $\phi(X)$ in the coalescence kernel ($E = 1.0$); (E) predicted histogram with $\epsilon(T)$ in the coalescence kernel ($\epsilon = 1.56 \times 10^{-3}$; $E = 0.32$); (V) predicted histogram with $\epsilon(T)$ and $\phi(X)$ in the coalescence kernel ($\epsilon = 0.49 \times 10^{-3}$; $\phi_a = 0.90$; $E = 0.13$). All histograms except (0) have the same dimensionless population.

sponds to the total number of particles, the area under a volume density curve represents the total volume of particles (Belval et al., 1984). Fig. 4 presents volume density data at an advanced stage of shear aggregation and compares this measurement with coalescence equation predictions. Note that aggregation in the shear field has generated aggregates comprising more than one thousand times the mean platelet volume. Again, calculated curve "V" does well in reproducing the observed histogram, even to the point of predicting the bimodal character of the observed volume density. As a rule, however, the coalescence equation predictions are not as accurate when extended to volume density comparisons.

AGGREGATION KINETICS EXPRESSED THROUGH ϵ AND ϕ

Our program of experiments examined the dependence of ϵ and ϕ on three experimental variables: shearing rate, platelet concentration, and time in the shear field. The experiments pertained to shear-induced aggregation in the absence of added chemical agonists.

Fig. 5 illustrates how the collision efficiency depends on the applied shearing rate for PRP suspensions receiving one minute exposure to the shear field. At shearing rates below 2,000 s^{-1}, the (time-average) collision efficiency is zero, indicating no net aggregation in the shear field. Above 2,000 s^{-1}, sustained aggregation occurs, as indicated by the nonzero values for ϵ. Moreover, ϵ rises between 2,000 s^{-1} and 5,000 s^{-1}, indicating that platelet activation in the shear field develops. At 10,000 s^{-1} there is a decline in the collision efficiency, although the extent of aggregation at this shearing rate was greatest. Between 5,000 s^{-1} and 10,000 s^{-1} the increase in particle collision frequency outstrips the increase in the extent of aggregation, reducing ϵ.

The collision efficiencies presented in Fig. 5, as time-average values for one minute in the shear field, do not provide information about the time course of ϵ. Fig. 6 describes how ϵ changes with time for the aggregation of PRP during the first minute in the shear field (G = 5,000 s^{-1}). During the first 10 s in the shear field, the time-averaging collision efficiency is $\sim 2.8 \times 10^{-3}$. However, over the next 20 s, ϵ has declined by two-thirds, to $\sim 1.0 \times 10^{-3}$. During the last 30 s, the collision efficiency remains at $\sim 1.0 \times 10^{-3}$.

Fig. 7 illustrates the strong dependence of the collision efficiency on platelet concentration. Here, the fraction of the suspension volume occupied by platelets, F, expresses the platelet concentration. The applied shearing rate is 5,000 s^{-1} for a period of 1 min. The four different curves represent experiments involving four different human subjects and illustrate the variability of platelet response among subjects. For all subjects, however, the collision efficiency declines as platelet suspensions become more dilute through the addition of autologous PFP until, below a threshold value of F, ϵ falls to zero, indicating no sustained aggregation. The extent of aggregation would be expected to be less in diluted platelet suspensions because of fewer particle collisions. However, Fig. 7 shows that the percentage of successful collisions also declines, until, below a threshold concentration, no aggregation occurs.

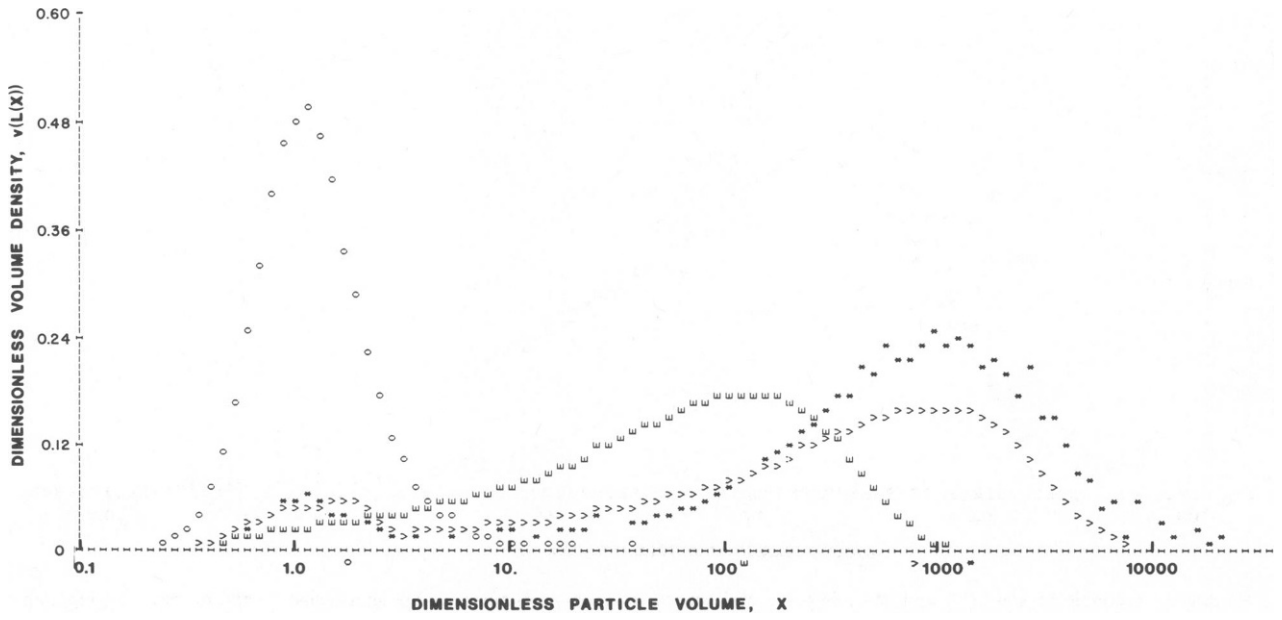

FIGURE 4 Comparison of observed and predicted volume density histograms at an advanced stage of shear aggregation (P = 0.15): (0) initial histogram for PRP; (*) histogram for PRP following 60 s exposure to G = 5,000 s^{-1}; (E) coalescence equation solution with $\epsilon(T)$ in the coalescence kernel ($\epsilon = 2.59 \times 10^{-3}$); ($V$) coalescence equation solution based on $\epsilon(T)$ and $\phi(X)$ in the coalescence kernel ($\epsilon = 1.17 \times 10^{-3}$; ϕ_a = 0.75). All histograms besides the initial histogram have the same dimensionless population.

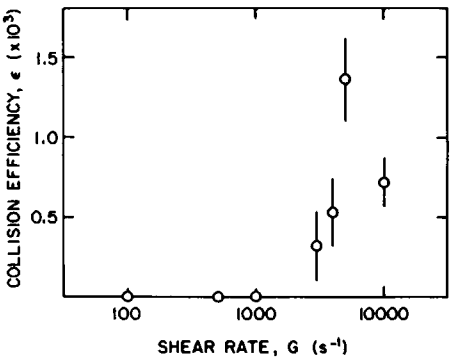

FIGURE 5 The dependence of the collision efficiency, ϵ, on shearing rate, G, for the shear aggregation of PRP, 60-s exposure to the shear field. The error bars represent 90% confidence interval estimates for the mean based on eight or more experiments with different human subjects.

On the average, this threshold is about $F = 0.0005$, equivalent to about 60,000 platelets per μl of suspension.

In contrast to the collision efficiency, the estimate for $\phi(X)$ was insensitive to either platelet concentration or the applied shearing rate. In most cases the choice for ϕ_a was 0.75. In a few cases $\phi_a = 0.90$ was the optimal value. Often, the histogram error was insensitive to ϕ_a between $0.75 \leq \phi_a \leq 0.975$. In the absence of a clear-cut optimal value for ϕ_a, we chose the smallest value among the candidates.

In the experiments involving a sequence of number density histograms over time, our choice for ϕ_a minimized the sum of the histogram errors across all time points. However, the optimal choice made this way often minimized the histogram error at each time point. Thus, the tacit assumption that ϕ is independent of time does not seem to introduce serious error.

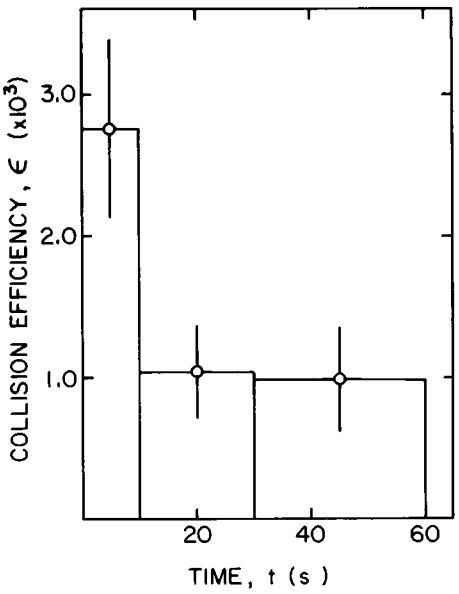

FIGURE 6 Decay of collision efficiency with elapsed time in the shear field for the shear aggregation of PRP at $G = 5{,}000\ s^{-1}$. Sampling times were at 10 s, 30 s, and 60 s. The error bars represent 90% confidence interval estimates for the mean based on ten or more experiments with different human subjects.

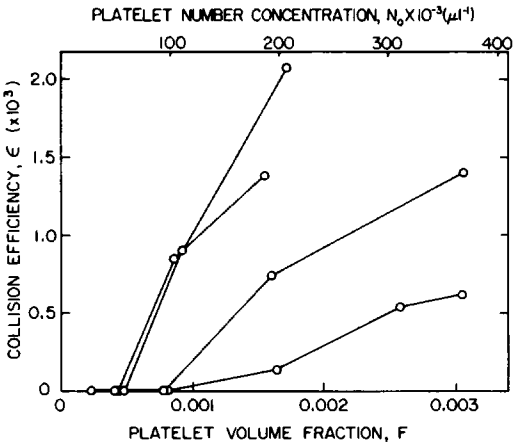

FIGURE 7 The decline in collision efficiency at lower platelet concentrations, for shear aggregation at $G = 5{,}000\ s^{-1}$ for 60 s. Each path represents an individual experiment wherein PRP was diluted by autologous PFP. The scale for N_0 assumes a mean platelet volume of 8 μm^3.

DISCUSSION

Comments on the Estimates for ϵ and ϕ

This paper presents a methodology for estimating particle collision efficiency, ϵ, and particle void volume fraction, ϕ, based on experimental measurements of particle number density for an aggregating collection of particles. For the shear aggregation of platelets, this technique produced an estimate for ϵ of $\sim 1 \times 10^{-3}$ and an estimate for ϕ of 0.75.

There are few relevant examples in the literature to compare against our estimate for ϵ. Swift and Friedlander (1964) calculated a collision efficiency of 0.4 for the coalescence of oil drops and the agglomeration of latex particles in laminar shearing flow at low shear rates. Chang and Robertson (1975) reported collision efficiencies up to 0.3 for the ADP-induced aggregation of rabbit platelets at low shear rates. Bell and Goldsmith (1984) obtained similar values for human platelets. These figures are two orders of magnitude higher than our estimate for the shear aggregation of platelets. However, our method gave similar estimates under similar circumstances: in pilot experiments, we obtained $\epsilon \sim 0.4$ for platelet aggregation at low shearing rates ($G < 500\ s^{-1}$) in response to added ADP. Other pilot experiments suggest that higher collision efficiencies may also result during shear aggregation if the shearing rate is reduced following an initial burst at a high shearing rate to activate the platelets. The low collision efficiency for shear aggregation, then, may be a consequence of the higher shearing rates employed, where collisions are more violent and forces acting to tear apart aggregates are greater. Optimum aggregation of activated platelets would appear to occur at low shear rates relative to the shear rates required to activate platelets.

No other investigators, to our knowledge, have attempted to estimate aggregate void volume fraction using a population balance approach. Born and Hume (1967) directly estimated the void fraction of platelet aggregates induced by ADP using a microscope. Their estimate places ϕ between 0.3 and 0.4 compared with our estimate of $\phi_a = 0.75$. Discounting the difference between ADP-induced and shear-induced aggregates, our higher estimate may arise from the effect of irregular particle shape on particle collision frequency. Evans and Proctor (1978) concluded from a theoretical analysis that irregular particle shape significantly inflates particle collision diameter in laminar shear aggregation. To achieve the same collision frequency as irregular particles our hypothetical spherical aggregates expand their collision diameter by enclosing more void space.

There is a similar complication in interpreting the values for ϵ. The estimate for ϵ implicitly assumes that no particle break-up occurs during shear aggregation. However, we have observed aggregate break-up at high shear rates over long exposure times as evidenced by an increase in the total particle count. As a result, our estimate for ϵ should be interpreted strictly as the collision efficiency for a hypothetical collection of particles that yield the same drop in population as the actual collection of particles, but where breakup does not occur.

Interpretation of Shear Aggregation

The appeal of population balance properties ϵ and ϕ is their close connection to physical aspects of particles pertinent to their aggregation behavior. The collision efficiency reflects the binding affinity of particles for one another. Platelets develop binding affinity as a consequence of their activation by physical and chemical stimuli. Collision efficiency estimates, then, offer a means of characterizing the activation of platelets in the shear field.

The connection between platelet activation and the collision efficiency allows further interpretation of the ϵ vs. G relationship depicted in Fig. 5. The upswing in ϵ between 2,000 s^{-1} and 5,000 s^{-1} suggests that platelet activation develops with increasing shear rate in this region. While the downturn in ϵ at 10,000 s^{-1} might result from a decline in activation, a more likely explanation is that the violent particle collisions at this extreme shear rate inhibit particle bindings. In addition, the shearing stress at such elevated shearing rates may tear apart existing aggregates, reducing the net number of particle bindings. Note that estimates for wall shear rates in parts of the human vasculature can approach 2,000 s^{-1} (Turritto and Baumgartner, 1982), the threshold we observed for platelet activation in the shear field.

Fig. 7 indicates that platelet activation in the shear field also depends on platelet concentration. The decline in collision efficiency in diluted platelet suspensions suggests that activation depends on a variable that changes with platelet concentration. One such variable is the concentration of chemicals (notably ADP) released or leaked from the granules of platelets exposed to shearing stress. Diluted platelet suspensions will have a proportionately smaller quantity of granule chemicals to offer the suspending medium. Perhaps platelets fail to become activated by the shear field if granule chemicals are not available in sufficient concentration. Based on data from Brown et al. (1975), the threshold platelet concentration in Fig. 7 could contribute only ~0.1 μM ADP to the plasma. This concentration is low when compared with ADP levels employed by Yung and Frojmovic (1982) and others to induce platelet aggregation in similar cone-plate viscometers.

The notion that platelet release (or leakage) of chemicals in the shear field mediates platelet activation is also consistent with the absence of shear aggregation below a threshold shearing rate of ~2,000 s^{-1}. Here, the platelet concentration is normal but the intensity of the shear field may not be adequate to induce sufficient release or leakage of granule chemicals. Other workers (Brown et al., 1975; Hardwick et al., 1983) have shown that the quantity of liberated chemicals (ADP, serotonin) increases with the applied shearing rate.

Thus, our interpretation of Fig. 7 supports an ADP-mediated mechanism for platelet activation in the shear field. This mechanism has been forwarded by other investigators (Moritz et al., 1983; Hardwick et al., 1983). Moritz demonstrated reduced shear aggregation in the presence of an enzyme system that consumes ADP. Hardwick obtained similar results using an agent (colchicine) that interferes with the platelet release reaction.

Gear (1982) has reported platelet aggregation in the first seconds after exposure to ADP. Our study indicates that shear-induced platelet aggregation also develops quickly. Platelet activation, however, begins to decay during the first minute in the shear field, even though aggregation continues. Fig. 6 shows the decay of platelet activation with time. Several different phenomena could explain the decay in binding affinity with time: (*a*) the platelets become refractory as exposure to the shear field continues; (*b*) more reactive platelets aggregate first, leaving less reactive members that aggregate more slowly, or; (*c*) aggregates begin to break apart as time proceeds, lowering the estimate for ϵ at later times. With regard to the third hypothesis, perhaps aggregates must reach a critical size before shearing forces begin to tear them apart. Additional experiments would be necessary before any of these possibilities could be excluded.

In summary, interpreting the kinetics of platelet aggregation in a shear field with a population balance, reveals a number of interesting points:

(*a*) During shear aggregation, only a small fraction of particle collisions in the shear field result in the binding together of the involved particles.

(*b*) The collision efficiency declines in diluted platelet suspensions, an observation supporting the hypothesis that

shear aggregation is mediated by the release or leakage of chemicals from platelets.

(*c*) The collision efficiency passes through a maximum with respect to shearing rate, suggesting a competition between two opposing influences: increasing platelet activation vs. increasing collision violence and other forces acting to destroy aggregates.

(*d*) The collision efficiency of platelets and aggregates decays with time in the shear field during shear aggregation.

(*e*) The collision efficiency is sensitive to the activating agonist and may prove to be a useful index to the state of activation of platelets.

The authors are indebted to Ms. Marcella Estrella and Mr. Clay Vernon for help in performing the experiments and interpreting data. We also thank Dr. Mary Wheeler for advice on numerical calculations and Dr. Jack Jen for numerous suggestions.

This research was supported by National Institutes of Health grants R01 HL 18584 and P01 NS 23327.

Received for publication 1 July 1985 and in final form 10 March 1986.

REFERENCES

Anderson, G. H., J. D. Hellums, J. L. Moake, and C. P. Alfrey. 1978*a*. Platelet lysis and aggregation in shear fields. *Blood Cells.* 4:499–507.

Anderson, G. H., J. D. Hellums, J. Moake, and C. P. Alfrey. 1978*b*. Platelet response to shear stress: changes in serotonin uptake, serotonin release, and ADP-induced aggregation. *Thromb. Res.*13:1039–1048.

Bell, D. N., and H. L. Goldsmith. 1984. Platelet aggregation in poiseuille flow: II effect of shear rate. *Microvasc. Res.* 27:316–330.

Belval, T. K. 1984. Population balance analysis of shear-induced platelet aggregation. Ph.D. thesis, Rice University. 178 pp.

Belval, T., J. D. Hellums, and R. T. Solis. 1984. The kinetics of platelet aggregation induced by fluid shearing stress. *Microvasc. Res.* 28:279–288.

Born, G. V. R., and M. Hume. 1967. Effects of the numbers and sizes of platelet aggregates on the optical density of plasma. *Nature (Lond.).* 215:1027–1029.

Brown, C. H., L. B. Leverett, C. W. Lewis, C. P. Alfrey, and J. D. Hellums. 1975. Morphological biochemical and functional changes in human platelets subjected to shear stress. *J. Lab. Clin. Med.* 86:462–471.

Chang, H. N., and C. R. Robertson. 1976. Platelet aggregation by laminar shear and Brownian motion. *Ann. Biomed. Eng.* 4:151–183.

Drake, R. L. 1972. A general mathematical survey of the coagulation equation. *In* Topics in Current Aerosol Research, part 2. G. M. Hidy and J. R. Brock, editors. Pergamon Press, Oxford. 201–376.

Evans, C. W., and J. Proctor. 1978. A collision analysis of lymphoid cell aggregation. *J. Cell Sci.* 33:17–36.

Frojmovic, M. M., and R. Panjwani. 1976. Geometry of normal mammalian platelets by quantitative microscopic studies. *Biophys. J.* 16:1071–1089.

Gear, A. R. L. 1982. Rapid reactions of platelets studied by a quenched-flow approach: aggregation kinetics. *J. Lab. Clin. Med.* 100:866–886.

Hardwick, R. A., H. N. Gritsman, R. R. Stromberg, and L. I. Friedman. 1983. The biochemical mechanism of shear-induced platelet aggregation. *Trans. Am. Soc. Artif. Intern. Organs.* 24:448–453.

Hellums, J. D., and R. A. Hardwick. 1981. Response of platelets to shear stress—a review. *In* The Rheology of Blood. D. R. Gross and N. H. C. Hwang, editors. Sijhoff and Noordhoff, Amsterdam. 160–183.

Johnston, G. G., U. Marzec, and E. F. Bernstein. 1975. Effects of surface injury and shear stress on platelet aggregation serotonin release. *Trans. Am. Soc. Artif. Intern. Organs.* 21:413–420.

Karino, T., and H. L. Goldsmith. 1979. Aggregation of human platelets in an annular vortex distal to a tubular expansion. *Microvasc. Res.* 17:217–237.

Martin, R. R., T. S. Dewitz, and L. V. Mcintire. 1979. Alterations in leukocyte structure and function due to mechanical trauma. *In* Quantitative cardiovascular studies. N. H. C. Hwang, D. R. Gross, and D. J. Patel, editors. University Park Press, Baltimore. 419–454.

Moritz, M. W., R. C. Reimers, R. K. Baker, S. P. Sutera, and J. H. Joist. 1983. Role of cytoplasmic and releasable ADP in platelet aggregation induced by laminar shear stress. *J. Lab. Clin. Med.* 101:537–544.

O'Rear E. A., M. M. Udden, L. V. McIntire, and E. C. Lynch. 1982. Reduced erythrocyte deformability associated with calcium accumulation. *Biochim. Biophys. Acta.* 691:274–280.

Paulus, J. M. 1975. Platelet size in man. *Blood.* 46:321–336.

Smoluchowski, M. V. 1917. Versuch einer mathematischen theorie der koagulations-kinetic kolloider losunger. *Z. Physik. Chem.* 92:129–168.

Swift, D. L., and S. K. Friedlander. 1964. The coagulation of hydrosols by Brownian motion and laminar shear flow. *J. Colloid. Sci.* 19:621–647.

Turritto, V. T., and H. R. Baumgartner. 1982. Platelet-surface interactions. *In* Hemostasis and Thrombosis—Basic Principles and Clinical Practice. R. W. Colman, J. Hirsh, V. J. Marder, and E. W. Salzman, editors. Lippincott, Philadelphia. 364–379.

Yung, W. and M. M. Frojmovic. 1982. Platelet aggregation in laminar flow I: adenosine diphosphate concentration, time, and shear rate dependence. *Thromb. Res.* 28:361–377.